Statics and dynamics of an Ashkin-Teller neural network with low loading

1998 J. Phys. A: Math. Gen. 31 6319

(http://iopscience.iop.org/0305-4470/31/30/002)

J. Phys. A: Math. Gen. **31** (1998) 6319–6332. Printed in the UK PII: S0305-4470(98)91183-0

Statics and dynamics of an Ashkin–Teller neural network with low loading

D Bollé† and P Kozłowski†‡
Instituut voor Theoretische Fysica, K U Leuven, B-3001 Leuven, Belgium

Received 30 January 1998, in final form 8 May 1998

Abstract. An Ashkin–Teller neural network, allowing for two types of neurons is considered in the case of low loading as a function of the strength of the respective couplings between these neurons. The storage and retrieval of embedded patterns built from the two types of neurons, with different degrees of (in)dependence is studied. In particular, thermodynamic properties including the existence and stability of Mattis states are discussed. Furthermore, the dynamic behaviour is examined by deriving flow equations for the macroscopic overlap. It is found that for *linked* patterns the model shows better retrieval properties than a corresponding Hopfield model.

1. Introduction

One of the best known physical models for neural networks is the Hopfield model [1]. In theoretical investigations of network properties, e.g. the retrieval of learned patterns, it plays a similar role as the Ising model does in the theory of magnetism. Extensions of this model to multistate neurons have received a lot of attention recently (see, e.g. [2–5] and the references cited therein). Thereby the ability to store and retrieve so-called grey-toned and coloured patterns has been investigated.

In this work we consider another extension of the Hopfield model to allow for multifunctional neurons. The specific model we have in mind is the neural network version of the Ashkin–Teller spin glass [6–9]. Indeed, on the one hand the Ashkin–Teller model has two different kinds of neurons (spins) at each site interacting with each other. This allows us to interprete this model as a neural network with two types of neurons having different functions. On the other hand, this Ashkin–Teller neural network (ATNN) can be considered as a model consisting of two interacting Hopfield models.

We expect the behaviour of the ATNN to be different from that of the Hopfield model in a nontrivial way. One of the things we want to find out, e.g. is whether this (four-neuron) interaction between the two types of neurons can improve the retrieval process for embedded patterns built from these two types of neurons. We shall see, indeed, that for a particular choice of this interaction term the retrieval quality of the embedded patterns is very high in comparison with a corresponding Hopfield model. Therefore, independent of the possible biological relevance of this model, if any, such a study is interesting from the pure physical point of view.

† Also at Interdisciplinair Centrum voor Neurale Netwerken, K U Leuven. E-mail address: desire.bolle@fys.kuleuven.ac.be
‡ Permanent address: Computational Physics Division, Institute of Physics, A Mickiewicz University, ul. Umultowska 85, PL 61-624 Poznań, Poland. E-mail address: piotr@tfdec1.fys.kuleuven.ac.be

0305-4470/98/306319+14$19.50

In this work we consider both the thermodynamic and dynamic properties of this model in the case of loading of a finite number of patterns.

The rest of this paper is organized as follows. In section 2 the ATNN model is introduced. Section 3 discusses the methods used for analysing both the equilibrium properties and the dynamics of the model. In particular, fixed-point equations as well as flow equations for the relevant macroscopic overlap order parameters are derived. In section 4 numerical solutions of these equations are discussed for a representative set of network parameters. The retrieval properties of embedded patterns with different degrees of dependences are compared. Section 5 presents the main conclusions.

2. The model

We consider a network of N sites. At each site we have two different types of binary neurons, s_i and σ_i, $i = 1, \ldots, N$. The two types of neurons interact via a four-neuron term $s_i s_j \sigma_i \sigma_j$. The infinite-range Hamiltonian reads

$$H = -\tfrac{1}{2} \sum_{i,j} [J_{ij}^{(1)} s_i s_j + J_{ij}^{(2)} \sigma_i \sigma_j + J_{ij}^{(3)} s_i s_j \sigma_i \sigma_j]. \tag{1}$$

In this network we wish to store a finite number of patterns, p, also of two different types, i.e. $\boldsymbol{\xi}_i = \{\xi_i^\mu\}$, $\mu = 1, \ldots, p$ and $\boldsymbol{\eta}_i = \{\eta_i^\nu\}$, $\nu = 1, \ldots, p$, which are supposed to be independent identically distributed random variables (i.i.d.r.v.) taking the values $+1$ or -1 with probability $\frac{1}{2}$. To build in the capacity for learning and retrieval in this network its stable configurations must be correlated with the configurations determined by the learning process. This can be accomplished by taking the Hebb learning rule for the interactions

$$J_{ij}^{(1)} = \frac{1}{N} J_1 \sum_{\mu=1}^{p} \xi_i^\mu \xi_j^\mu \qquad J_{ij}^{(2)} = \frac{1}{N} J_1 \sum_{\mu=1}^{p} \eta_i^\mu \eta_j^\mu \qquad J_{ij}^{(3)} = \frac{1}{N} J_3 \sum_{\mu=1}^{p} \gamma_i^\mu \gamma_j^\mu \tag{2}$$

where the $\boldsymbol{\gamma}_i = \{\gamma_i^\mu\}, \mu = 1, \ldots, p$ are also i.i.d.r.v. taking the values $+1$ or -1 with probability $\frac{1}{2}$.

At this point some remarks are in order. First, we have taken the strength of the two types of patterns to be equal, meaning that the ATNN model is isotropic. Second, it is clear that the behaviour of this model (1), (2) might depend on whether the $\boldsymbol{\gamma}$ are taken to be independent from the $\boldsymbol{\xi}$ and the $\boldsymbol{\eta}$ or not. The following cases will be distinguished:

(1) unlinked patterns

(a) $\boldsymbol{\xi}_i, \boldsymbol{\eta}_i$ and $\boldsymbol{\gamma}_i$ are i.i.d.r.v.

(b) $\boldsymbol{\xi}_i = \boldsymbol{\eta}_i$ and $\boldsymbol{\gamma}_i$ are i.i.d.r.v.

(c) $\boldsymbol{\xi}_i = \boldsymbol{\eta}_i = \boldsymbol{\gamma}_i$ is i.i.d.r.v.

(2) linked patterns

$\gamma_i^\mu = \xi_i^\mu \eta_i^\mu$ with $\boldsymbol{\xi}_i$ and $\boldsymbol{\eta}_i$ are i.i.d.r.v.

We note that this ATNN model can also be considered as an assembly of two single Hopfield models (when $J_3 = 0$), one in the s_i-neurons and one in the σ_i-neurons interconnected via a four-neuron interaction (when $J_3 \neq 0$). The study of coupled Hopfield networks has aroused some interest in the literature before (e.g. [10]).

In the following we discuss both the thermodynamics and the dynamics of this ATNN neural network with low loading.

3. The method

3.1. Statics

Starting from the Hamiltonian (1), (2) and applying standard techniques (linearization and the saddle-point method [11, 12]) the ensemble-averaged free energy is given by

$$f = \tfrac{1}{2}(J_1\boldsymbol{m}_1^2 + J_1\boldsymbol{m}_2^2 + J_3\boldsymbol{m}_3^2) - \frac{1}{\beta}\langle\!\langle \ln[4\cosh\beta L_1\cosh\beta L_2\cosh\beta L_3(1+\tanh\beta L_1\tanh\beta L_2\tanh\beta L_3)]\rangle\!\rangle \tag{3}$$

with

$$L_1 = J_1\boldsymbol{\xi}\cdot\boldsymbol{m}_1 \qquad L_2 = J_1\boldsymbol{\eta}\cdot\boldsymbol{m}_2 \qquad L_3 = J_3\boldsymbol{\gamma}\cdot\boldsymbol{m}_3. \tag{4}$$

In the above the double brackets $\langle\!\langle\cdot\rangle\!\rangle$ denote the average over the distribution of the embedded patterns. The $\boldsymbol{m}_\alpha = \{m_\alpha^\mu\}$, $\mu = 1,\ldots,p$; $\alpha = 1,2,3$ are, as usual, overlap order parameters defined by

$$\boldsymbol{m}_1 = \frac{1}{N}\sum_{i=1}^{N}\boldsymbol{\xi}_i s_i \qquad \boldsymbol{m}_2 = \frac{1}{N}\sum_{i=1}^{N}\boldsymbol{\eta}_i\sigma_i \qquad \boldsymbol{m}_3 = \frac{1}{N}\sum_{i=1}^{N}\boldsymbol{\gamma}_i s_i\sigma_i. \tag{5}$$

Here we remark that in the thermodynamic limit $N\to\infty$ and for finite loading $\alpha = 0$ the diagonal terms in the couplings, J_{ii}, do not play any role in the Hamiltonian (1).

In fact our model can be considered as a special case of the general spin-glass model presented in [8] such that the expressions (3), (4) can also be read off from there.

The fixed-point equations for the order parameters read

$$\boldsymbol{m}_\alpha = \left\langle\!\!\left\langle \frac{\boldsymbol{\psi}_\alpha(\tanh\beta L_\alpha + \tanh\beta L_\nu\tanh\beta L_\rho)}{1+\tanh\beta L_\alpha\tanh\beta L_\nu\tanh\beta L_\rho}\right\rangle\!\!\right\rangle \tag{6}$$

where $\alpha,\nu,\rho = 1,2,3$ are taken to be different and where $\boldsymbol{\psi}_\alpha$ is the embedded pattern corresponding to $\boldsymbol{m}_\alpha$.

Since the study of this ATNN model is very involved we have restricted ourselves here to a detailed treatment of the Mattis states [12] which are especially important from a neural network point of view. In our case they are defined as those solutions of the fixed-point equations for which not more than one component of each order parameter is different from zero, e.g. $\boldsymbol{m}_1 = m_1(1,0,\ldots,0)$, $\boldsymbol{m}_2 = m_2(1,0,\ldots,0)$, $\boldsymbol{m}_3 = m_3(1,0,\ldots,0)$. These states are denoted by $m_1m_2m_3$ in the following. We will see that those states are the only ones which contribute to the thermodynamics of the system. Solutions with more than one component being nonzero, i.e. mixture states will be important for the dynamics if they are local minima of the free energy.

For zero temperature we note that the equations (6) can be simplified by replacing the $\tanh\beta L_\alpha$ by $\operatorname{sign} L_\alpha$. Then it is straightforward to show that for each order parameter

$$(\boldsymbol{m}_\alpha)^2 \leqslant 1 \qquad \alpha = 1,2,3 \tag{7}$$

with the equality being satisfied for a one-component $\boldsymbol{m}_\alpha$, and that the ground-state energy is given by

$$E = -\sum_{\alpha=1}^{3}\tfrac{1}{2}\boldsymbol{m}_\alpha^2. \tag{8}$$

In section 4 we report on the existence and stability of these Mattis states as a function of the temperature.

3.2. Dynamics

The analysis outlined above enables us to find the local minima of the free energy, but in order to find out how an arbitrary initial state of the network changes in time and to what extent, if at all, one of the learned patterns is approached, we derive a flow equation for the overlap order parameters.

We consider sequential updating of the spins consistent with the detailed balance condition. Hence we choose the following transition probabilities for a spin–flip at a certain time step

$$\begin{aligned}
\omega_1(s_i,\sigma_i) &\equiv \omega(s_i \to -s_i) = \tfrac{1}{12}[1-\tanh(\beta(s_i h_i^{(1)} + s_i\sigma_i h_i^{(3)}))] \\
\omega_2(s_i,\sigma_i) &\equiv \omega(\sigma_i \to -\sigma_i) = \tfrac{1}{12}[1-\tanh(\beta(\sigma_i h_i^{(2)} + s_i\sigma_i h_i^{(3)}))] \\
\omega_3(s_i,\sigma_i) &\equiv \omega(s_i \to -s_i, \sigma_i \to -\sigma_i) = \tfrac{1}{12}[1-\tanh(\beta(s_i h_i^{(1)} + \sigma_i h_i^{(2)}))]
\end{aligned} \tag{9}$$

with the h_i appropriate local fields acting on the neurons in the following way

$$h_i^{(1)} = \frac{J_1}{N}\sum_j\sum_\mu \xi_i^\mu \xi_j^\mu s_j \qquad h_i^{(2)} = \frac{J_2}{N}\sum_j\sum_\mu \eta_i^\mu \eta_j^\mu \sigma_j \qquad h_i^{(3)} = \frac{J_3}{N}\sum_j\sum_\mu \gamma_i^\mu \gamma_j^\mu s_j\sigma_j \tag{10}$$

where, as in the treatment of the statics we take $J_1 = J_2$. At this point we remark that in the thermodynamic limit $N \to \infty$ the diagonal terms in the couplings, J_{ii}, do not survive. Furthermore we note that the method used here is also valid in the case of unequal J.

We then consider the probability $p(\boldsymbol{s},\boldsymbol{\sigma};t)$ that the system is in a state $\boldsymbol{s} = (s_i,\ldots,s_N)$, $\boldsymbol{\sigma} = (\sigma_1,\ldots,\sigma_N)$ at time t. It satisfies the master equation

$$\begin{aligned}
\frac{\partial p(\boldsymbol{s},\boldsymbol{\sigma};t)}{\partial t} = \sum_{i=1}^N \{&\omega_1(F_i^1 s_i,\sigma_i)p(F_i^1\{\boldsymbol{s},\boldsymbol{\sigma}\};t) + \omega_2(s_i,F_i^2\sigma_i)p(F_i^2\{\boldsymbol{s},\boldsymbol{\sigma}\};t) \\
&+\omega_3(F_i^3 s_i,F_i^3\sigma_i)p(F_i^3\{\boldsymbol{s},\boldsymbol{\sigma}\};t) \\
&-p(\boldsymbol{s},\boldsymbol{\sigma};t)[\omega_1(s_i,\sigma_i)+\omega_2(s_i,\sigma_i)+\omega_3(s_i,\sigma_i)]\}.
\end{aligned} \tag{11}$$

The operator F_i^ν, $\nu = 1,2,3$ acting on a configuration $\{\boldsymbol{s},\boldsymbol{\sigma}\}$ changes the sign of the following spins: s_i for $\nu = 1$, σ_i for $\nu = 2$ and simultaneously s_i and σ_i for $\nu = 3$.

From this we wish to derive a flow equation for the overlap order parameters. Because of the multistate character of the model (owing to the four-spin interaction term) the summation over i has to be carried out by generalizing the method of submagnetizations or suboverlaps connected with partitions of the network with respect to the built-in patterns [13, 14]. We note that for Hopfield networks we do not need such a partitioning [15].

First we introduce the following division of the network indices

$$\{i \leqslant N\} = \bigcup_{\boldsymbol{k}} I_{\boldsymbol{k}} \qquad I_{\boldsymbol{k}} = \{i \leqslant N; \boldsymbol{k} = \boldsymbol{k}_i\} \qquad \boldsymbol{k}_i = (\boldsymbol{\xi}_i,\boldsymbol{\eta}_i,\boldsymbol{\gamma}_i). \tag{12}$$

Then we define the so-called submagnetizations or suboverlaps

$$\mu_{\alpha,\boldsymbol{k}}(\boldsymbol{s},\boldsymbol{\sigma}) = \frac{1}{|I_{\boldsymbol{k}}|}\sum_{i\in I_{\boldsymbol{k}}} S_{\alpha,i} \qquad \alpha = 1,2,3,\ \ S_{1,i} = s_i,\ \ S_{2,i} = \sigma_i,\ \ S_{3,i} = s_i\sigma_i \tag{13}$$

which enables us to write the overlaps in the form

$$m_\alpha^\nu = \sum_{\boldsymbol{k}} \frac{|I_{\boldsymbol{k}}|}{N}\mu_{\alpha,\boldsymbol{k}} k^{(\alpha-1)p+\nu} \qquad \alpha = 1,2,3,\ \ \nu = 1,\ldots,p \tag{14}$$

where $|I_k|$ stands for the number of indices in the set I_k. The number of vectors $\boldsymbol{k}$ is equal to 2^{ap}, which is much smaller than the number N of sites i (when $N \to \infty$). The coefficient

$a = 3, 2, 1$ and 2 for patterns of type 1(a), 1(b), 1(c) and 2 respectively. So, an embedded random pattern configuration can be assumed to be equally distributed over the sets I_k such that $|I_k| = 2^{-ap}N + \mathcal{O}(N^{1/2})$.

Next we write down the probability $P(\boldsymbol{\mu}; t)$ that the system is in a macroscopic state described by a set of submagnetizations $\boldsymbol{\mu}(\boldsymbol{s}, \boldsymbol{\sigma}) \equiv \{\mu_{\alpha,k}\}$

$$P(\boldsymbol{\mu}; t) = \sum_{\{\boldsymbol{s},\boldsymbol{\sigma}\}} p(\boldsymbol{s}, \boldsymbol{\sigma}; t)\delta(\boldsymbol{\mu} - \boldsymbol{\mu}(\boldsymbol{s}, \boldsymbol{\sigma})). \tag{15}$$

Then we arrive at the following master equation (cf equation (11))

$$\frac{\partial P(\boldsymbol{\mu}; t)}{\partial t} = \sum_{\{\boldsymbol{s},\boldsymbol{\sigma}\}} \sum_i \sum_\nu \omega_\nu(s_i, \sigma_i) p_t(\boldsymbol{s}, \boldsymbol{\sigma})[\delta(\boldsymbol{\mu} - \boldsymbol{\mu}(F_i^\nu\{\boldsymbol{s}, \boldsymbol{\sigma}\})) - \delta(\boldsymbol{\mu} - \boldsymbol{\mu}(\boldsymbol{s}, \boldsymbol{\sigma}))]. \tag{16}$$

The action of the operator F_i^ν can be specified further by writing

$$\boldsymbol{\mu}(F_i^\nu\{\boldsymbol{s}, \boldsymbol{\sigma}\}) = \boldsymbol{\mu}(\boldsymbol{s}, \boldsymbol{\sigma}) - \boldsymbol{R}^\nu(s_i, \sigma_i). \tag{17}$$

It is then straightforward to check that certain elements of the matrix $[\boldsymbol{R}^\nu(s_i, \sigma_i)]_{\alpha,k}$ are zero, namely

$$R^1_{2,k} = R^2_{1,k} = R^3_{3,k} = 0 \qquad \forall k,\ i \leqslant N. \tag{18}$$

Furthermore, for ν and α different from these specific values in (18) we have

$$R^\nu_{\alpha,k} = \frac{2}{|I_k|} S_{\alpha,i} \qquad \text{if } i \in I_k \tag{19}$$

$$R^\nu_{\alpha,k} = 0 \qquad \text{if } i \notin I_k. \tag{20}$$

In the thermodynamic limit $N \to \infty$ the parameters $\boldsymbol{\mu}$ become continuous variables. Following [13] we then write for an arbitrary smooth function $\phi(\boldsymbol{\mu})$

$$\begin{aligned}\frac{\partial\langle\phi(t)\rangle}{\partial t} &\equiv \int \mathrm{d}\boldsymbol{\mu}\, \phi(\boldsymbol{\mu}) \frac{\partial P(\boldsymbol{\mu}; t)}{\partial t} \\ &= \sum_{\{\boldsymbol{s},\boldsymbol{\sigma}\}} \sum_i \sum_\nu \int \mathrm{d}\boldsymbol{\mu}'\, p(\boldsymbol{s}, \boldsymbol{\sigma}; t)\delta(\boldsymbol{\mu}' - \boldsymbol{\mu}(\boldsymbol{s}, \boldsymbol{\sigma}))\omega_\nu(s_i, \sigma_i) \\ &\quad \times[\phi(\boldsymbol{\mu}' - \boldsymbol{R}^\nu(s_i, \sigma_i)) - \phi(\boldsymbol{\mu}')].\end{aligned} \tag{21}$$

Making an expansion of ϕ around $\boldsymbol{\mu}'$ and doing a partial integration with respect to $\boldsymbol{\mu}'$ we arrive at

$$\begin{aligned}\frac{\partial\langle\phi(t)\rangle}{\partial t} = \int \mathrm{d}\boldsymbol{\mu}'\, \phi(\boldsymbol{\mu}') \sum_{\alpha,k} \frac{\partial}{\partial \mu'_{\alpha,k}} \Bigg(&\sum_{\{\boldsymbol{s},\boldsymbol{\sigma}\}} \sum_i \sum_\nu p(\boldsymbol{s}, \boldsymbol{\sigma}; t)\delta(\boldsymbol{\mu}' - \boldsymbol{\mu}(\boldsymbol{s}, \boldsymbol{\sigma})) \\ &\times R^\nu_{\alpha,k}(s_i, \sigma_i)\omega_\nu(s_i, \sigma_i)\Bigg) + \mathcal{O}(N^{-1}).\end{aligned} \tag{22}$$

We remark that until now we have not used the specific form for the transition probabilities ω_ν. Other expressions for ω_ν, satisfying detailed balance could also be employed.

Using the partitioning of the network into subsets I_k we can replace the sum over i by $\sum_k \sum_{i \in I_k}$. Employing the specific form (9) for ω_ν and performing the sum over $\{\boldsymbol{s}, \boldsymbol{\sigma}\}$ we arrive at (cf [13])

$$\frac{\partial\langle\phi\rangle_t}{\partial t} = \int \mathrm{d}\boldsymbol{\mu}\, \phi(\boldsymbol{\mu}) \sum_{\alpha,k} \frac{\partial}{\partial \mu_{\alpha,k}} P(\boldsymbol{\mu}; t)[\tfrac{1}{3}\mu_{\alpha,k} - f_{\alpha,k}(\{\mu_{\beta,k}\})] \tag{23}$$

where $f_{\alpha,\boldsymbol{k}}(\{\mu_{\beta,\boldsymbol{k}}\})$ is a function of all the suboverlaps given by

$$\begin{aligned} f_{\alpha,\boldsymbol{k}}(\{\mu_{\beta,\boldsymbol{k}}\}) = \tfrac{1}{12}\{&\tanh(\beta L_\alpha + \beta L_\nu) + \tanh(\beta L_\alpha - \beta L_\nu) + \tanh(\beta L_\alpha + \beta L_\rho) \\ &+ \tanh(\beta L_\alpha - \beta L_\rho) + \mu_{\nu,\boldsymbol{k}}[\tanh(\beta L_\alpha + \beta L_\rho) - \tanh(\beta L_\alpha - \beta L_\rho)] \\ &+ \mu_{\rho,\boldsymbol{k}}[\tanh(\beta L_\alpha + \beta L_\nu) - \tanh(\beta L_\alpha - \beta L_\nu)]\} \end{aligned} \tag{24}$$

with the L_α ($\alpha, \nu, \rho = 1, 2, 3$ and different from each other) given by equation (4). Since this equation holds for every smooth function ϕ the equation for the probabilities $P(\boldsymbol{\mu}; t)$ has the form

$$\frac{\partial P(\boldsymbol{\mu}; t)}{\partial t} = \sum_{\alpha,\boldsymbol{k}} \frac{\partial}{\partial \mu_{\alpha,\boldsymbol{k}}} P(\boldsymbol{\mu}; t)[\tfrac{1}{3}\mu_{\alpha,\boldsymbol{k}} - f_{\alpha,\boldsymbol{k}}(\{\mu_{\beta,\boldsymbol{k}}\})] \tag{25}$$

and the corresponding flow equations for the submagnetizations $\mu_{\alpha,\boldsymbol{k}}$ themselves read

$$\frac{\partial \mu_{\alpha,\boldsymbol{k}}}{\partial t} = -\tfrac{1}{3}\mu_{\alpha,\boldsymbol{k}} + f_{\alpha,\boldsymbol{k}}(\{\mu_{\beta,\boldsymbol{k}}\}). \tag{26}$$

Together with (14) these coupled equations are used to study the dynamic behaviour of the network. In the following section the results of this study are discussed.

4. Results

In this section we discuss the numerical results for the ATNN model obtained from the fixed-point equations specifying the thermodynamic properties and from the flow equations for the suboverlaps describing the dynamics. We treat the cases of linked patterns and unlinked patterns separately. We report the results for a set of representative examples illustrating the main new features of the model.

4.1. Unlinked patterns

We first consider the model with equal coupling parameters $J_3 = J_1 (= J_2) = 1$. Introducing Mattis-type states $m_1 m_2 m_3$ into the fixed-point equations (6) we obtain the same equations for $\boldsymbol{m}_\alpha$, $\alpha = 1, 2, 3$ irrespective of the degree of dependence between the different types of patterns. The solutions are presented in figure 1 where the overlap for different Mattis states is shown as a function of the temperature $T = 1/\beta$. A stability analysis performed by studying the stability matrix given by $\mathrm{A}^{\mu\nu}_{\alpha\beta} = \frac{\partial^2 f}{\partial m^\mu_\alpha \partial m^\nu_\beta}$ leads to the following main features. Above $T = 1.0$ there exist no stable Mattis states. Furthermore, the (paramagnetic) state 000 where all the overlaps with the embedded patterns are zero is stable.

Below $T = 1.0$ we have the retrieval phase with many different forms of stable Mattis states. We expect that the most important ones are those with the lowest energies, i.e. the states mmm (for temperatures in the interval $(0.83, 1)$) and $mm0$ (for temperatures in $(0, 0.83)$). The state $mm0$ corresponds to a situation where the overlaps with a pattern in the s-part and σ-part of the network are nonzero and equal to each other and the overlap with a pattern in the $s\sigma$-part of the network is zero. This state is completely equivalent to the states $m0m$ and $0mm$, a fact resulting directly from the symmetry of the model. Its properties are analogous to those of the Mattis states in the Hopfield model [12], since the fixed-point equations for the overlap m are the same.

The states which have no analogues in the Hopfield model are mmm and also mml. The first can be interpreted as the description of retrieval of one pattern, 'simultaneously by the s, σ and $s\sigma$-parts of the network' (for the case of dependent patterns, i.e. case 1(c), this pattern is the same for the three parts). However, such a retrieval occurs with a lot of

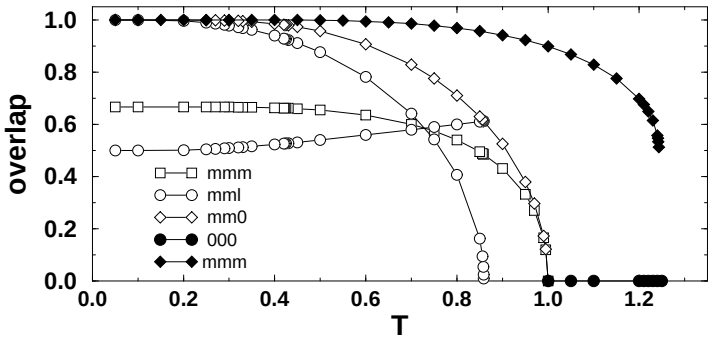

Figure 1. The overlaps for the Mattis states as a function of the temperature $T = 1/\beta$ for $J_1 = J_2 = J_3 = 1$. States represented by filled symbols are only present for the model with linked patterns.

errors as can be inferred from the small values of the corresponding overlap in figure 1. The second state, i.e. *mml*, which is, of course, equivalent to *mlm* and *lmm* differs from the *mmm* state in the fact that the nonzero overlaps with the pattern in the three different parts of the network are not equal to each other. However, this state does not seem to play an important role because it is never a global minimum in the set of Mattis states (see figure 1).

Increasing the temperature to $T = 1$ we notice a continuous transition from the network retrieval phase to the disordered (paramagnetic) phase.

We have also studied the local minima structure for nonequal values of the coupling parameters J_1, J_2 and J_3. It only differs in a quantitative way.

The static results found above are confirmed by a study of the dynamic behaviour of the ATNN model using the coupled equations (26). For simplicity, we take the number of embedded patterns of each type $p = 2$. Since we have three different kinds of such patterns the results concern a six-dimensional flow. Some representative two-dimensional projections are presented in figure 2.

As a starting point we take $\boldsymbol{m}_2 = \boldsymbol{m}_3 = (0.5, 0)$ and different values for $\boldsymbol{m}_1$. Such a choice of initial conditions is not very specific because of the symmetry properties of the model. It allows us to show some typical behaviour of the network. An extensive search confirms that other initial conditions lead only to quantitatively different diagrams. We remark that the part of the diagrams not shown explicitly is symmetric with respect to the m_1^1 or m_1^2 axis.

We choose some relevant values of T suggested by the thermodynamics. We can locate in the first diagram of figure 2 ($T = 0.1$) the attractor $0mm$ in the lower left corner. In the lower right (and, since there is symmetry with respect to the off-diagonal also the upper left) corner we see the state *lmm*, which looks like an attractor. However, our static analysis reveals that they are only saddle points in the full six-dimensional space. On the off-diagonal we have a state of the form $\boldsymbol{m}_1 = m_1(1, 1)$, $\boldsymbol{m}_2 = m_2(1, 0)$ and $\boldsymbol{m}_3 = m_3(1, 0)$ denoted by *smm*, i.e. symmetric with respect to the *s*-part of the network. We remark that in this diagram some lines cross each other which is caused by the fact that only the evolution of two order parameters is shown whereas the third order parameter, $m_2^1 = m_3^1$, is also evolving. One could easily imagine a three-dimensional picture with $m_2^1 = m_3^1$ taken as the third coordinate.

For increasing T the *smm* state is no longer present and the *lmm* states move along

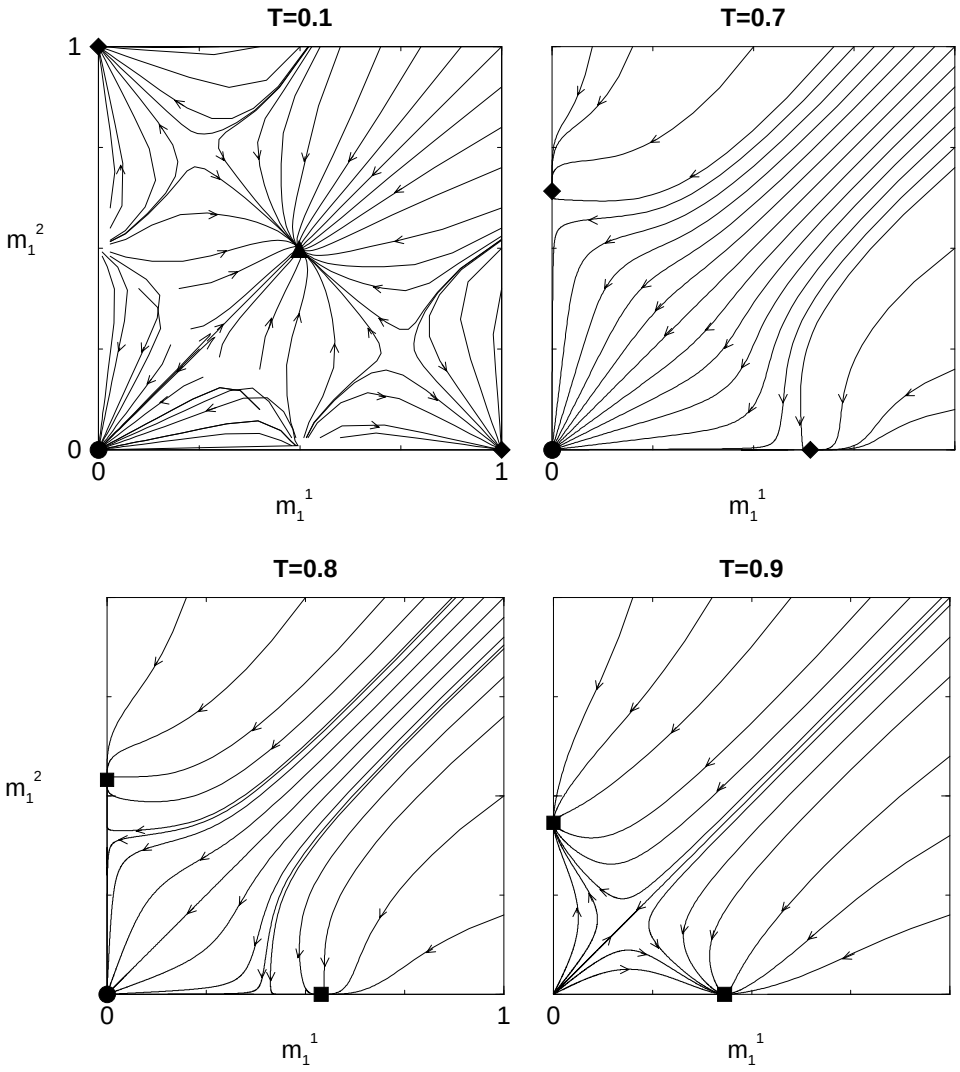

Figure 2. Flow diagrams for the model with unlinked patterns at several temperatures. Filled symbols denote different states: a circle for 0*mm*, a diamond for *lmm*, a square for *mmm* and a triangle for the symmetric state *smm* defined in the text.

the m_1^1-axis (respectively m_1^2-axis) until they disappear for $T \approx 0.8$. For these temperatures there is a very small difference in free energy between the various Mattis-type states. This could be the reason that for $T = 0.8$ we were no longer able to detect the states *lmm* which should still exist according to the static analysis. Indeed, at this temperature the overlap for the *lmm* states is almost equal to the one for the *mmm* state (see figure 1) showing that they are almost identical. Furthermore, for $T \approx 0.8$ the states *mmm* appear, move towards the origin on the m_1^1-axis (respectively the m_1^2-axis) as seen on the diagram for $T = 0.9$ and disappear for $T = 1.0$. From this temperature onwards, only the origin, i.e. the 000 state is an attractor.

4.2. Linked patterns

Next, we have analysed the model with linked patterns satisfying $\gamma^\mu = \xi^\mu \eta^\mu$ with $\boldsymbol{\xi}$ and $\boldsymbol{\eta}$ i.i.d.r.v. and with equal coupling parameters $J_3 = J_1 (= J_2) = 1$.

Introducing again Mattis-type states $m_1 m_2 m_3$ into the fixed-point equations (6) and checking their stability we find that there are only two stable solutions: the retrieval state mmm which is stable below $T = 1.213$ and the paramagnetic 000 state which is stable above $T = 1.0$. The corresponding retrieval overlap is shown in figure 1 (filled symbols). We notice that in contrast to the model with unlinked patterns a state of the form mmm has a much bigger overlap.

Hence, we can distinguish different phases: a retrieval phase below $T = 1.213$ and a paramagnetic phase above $T = 1.213$. We remark that the transition at $T = 1.213$ is first order. In the temperature region $1 \leqslant T < 1.213$ both the paramagnetic and Mattis solutions are local minima of the free energy. Such a region has also been seen in the Potts model but not in the Hopfield model [13]. Finally, we find that Hopfield-type solutions, i.e. Mattis states of the form $m00$ are (only) saddle points below $T = 1.0$.

A detailed study of the flow equations (26) reveals a much more complicated local minima structure for this model. It turns out that for the model with linked patterns we still have to distinguish between the Mattis solutions according to the relative place of the nonzero overlap components for the different order parameters. Consequently, we introduce *simple* Mattis states where only the same components of the different order parameters are nonzero, e.g. $\boldsymbol{m}_1 = m_1(1, 0)$, $\boldsymbol{m}_2 = m_2(1, 0)$, and $\boldsymbol{m}_3 = m_3(1, 0)$ for $p = 2$, denoted as before by $m_1 m_2 m_3$. For equal components m_α these are the states we have encountered in the thermodynamic analysis. (They are equivalent to $(0, m)(0, m)(0, m)$ and also to $(-m, 0)(-m, 0)(m, 0)$.)

In addition, we define *crossed* Mattis states where the same components of the different order parameters are never nonzero, e.g. $(m, 0)(0, m)(0, 0)$ for $p = 2$ and $(m, 0, 0)(0, m, 0)(0, 0, m)$ for $p = 3$. At this point we remark that a state of the form $(m, 0)(0, m)(m, 0)$ is neither simple nor crossed but of a mixed form. For $p = 2$ we did not detect the latter. The crossed states are in fact equivalent to Mattis states for a model with unlinked patterns. This can easily be checked by introducing this type of solutions in the fixed-point equations for the order parameters and taking appropriate averages over the linked patterns.

Some representative flow diagrams are shown in figures 3 and 4. As before we present only projections onto a two-dimensional space. The symmetry of the model with linked patterns is different from the model with unlinked patterns which results in a different symmetry of the flow diagrams. So, the remaining part of a diagram in these figures can be obtained by a reflection of the part displayed with respect to the axis $m_1^2 = 0$.

The initial conditions for the flow diagrams of figure 3 are as follows: two identical Mattis states with $\boldsymbol{m}_2 = \boldsymbol{m}_3 = (0.5, 0)$. We can locate in the first diagram of figure 3 ($T = 0.1$) the attractor mmm in the lower right corner. In the lower left corner we see the state $m00$, which again looks like an attractor. However, it is only a saddle point in the full six-dimensional space. On the top in the middle we have a state of the form $\boldsymbol{m}_1 = (m_1^1, m_1^2)$, $\boldsymbol{m}_2 = m_2(1, 0)$ and $\boldsymbol{m}_3 = m_3(1, 0)$ denoted by amm, i.e. asymmetric with respect to the s-part of the network. We remark also that any crossings of paths are caused by the fact that the diagrams of figure 3 and also of figure 4 are projections of a higher dimensional flow. They are not present in the full six-dimensional space.

For higher T the state amm disappears, the state mmm stays in the lower right corner up to $T = 1$ and the state $m00$ moves towards the origin and disappears at $T = 1$. Above

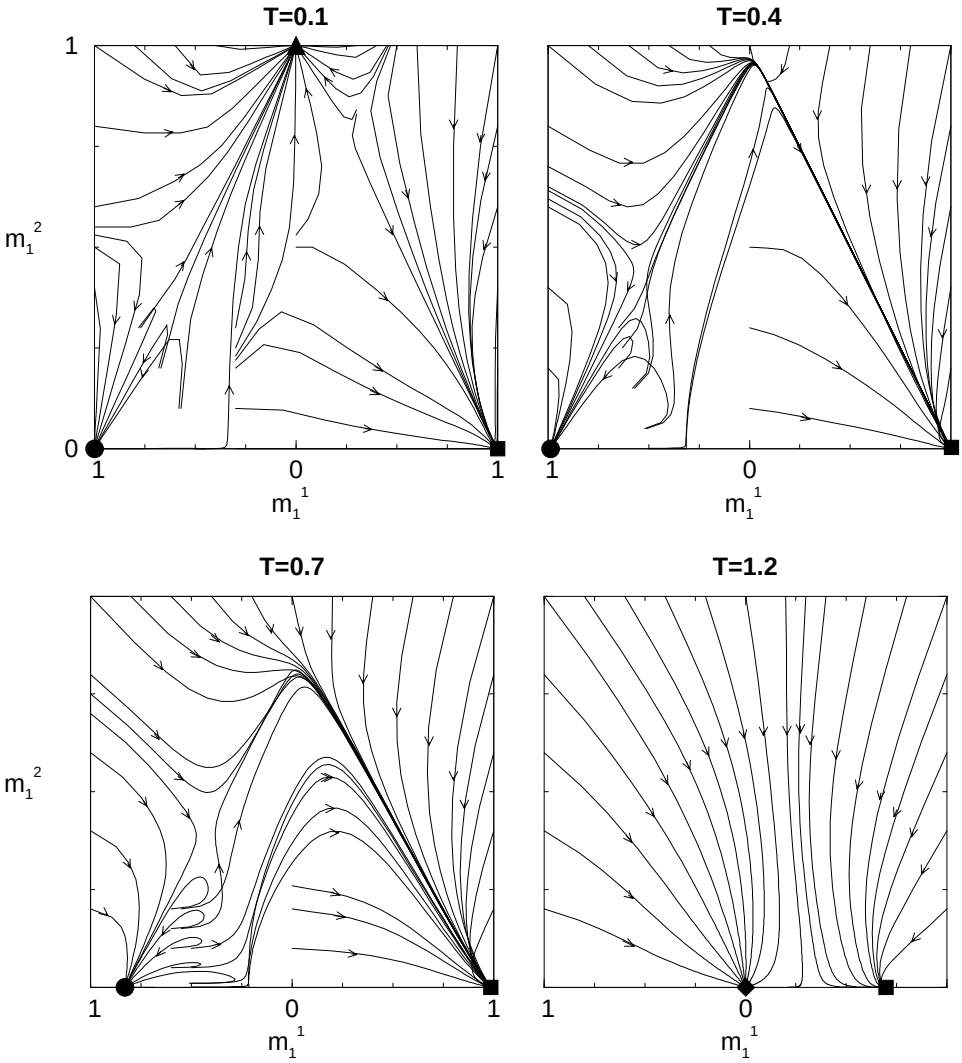

Figure 3. Flow diagrams for the model with linked patterns at different temperatures. Filled symbols stand for different states: a circle for $m00$, a square for mmm, a diamond for 000 and a triangle for the asymmetric state amm defined in the text.

$T = 1$ (see the diagram for $T = 1.2$) both the origin and the state mmm are stable, but the latter has already moved towards the origin. We note that in contrast to the model with unlinked patterns, it does not reach the origin since the transition (to the paramagnetic phase) is first order.

Another illustrative set of diagrams is presented in figure 4. Here the initial conditions are more general: $\boldsymbol{m}_2 = (0.1, 0)$, $\boldsymbol{m}_3 = (0.5, 0.0)$. In the first diagram for $T = 0.1$ an attractor mmm is present in the lower left and right corners. On the top in the middle the state $mm0$ is located. It is a crossed state and a minimum at low temperatures. The overlap m in this state depends on T in the same way as the overlap of a Mattis solution of the standard Hopfield model does.

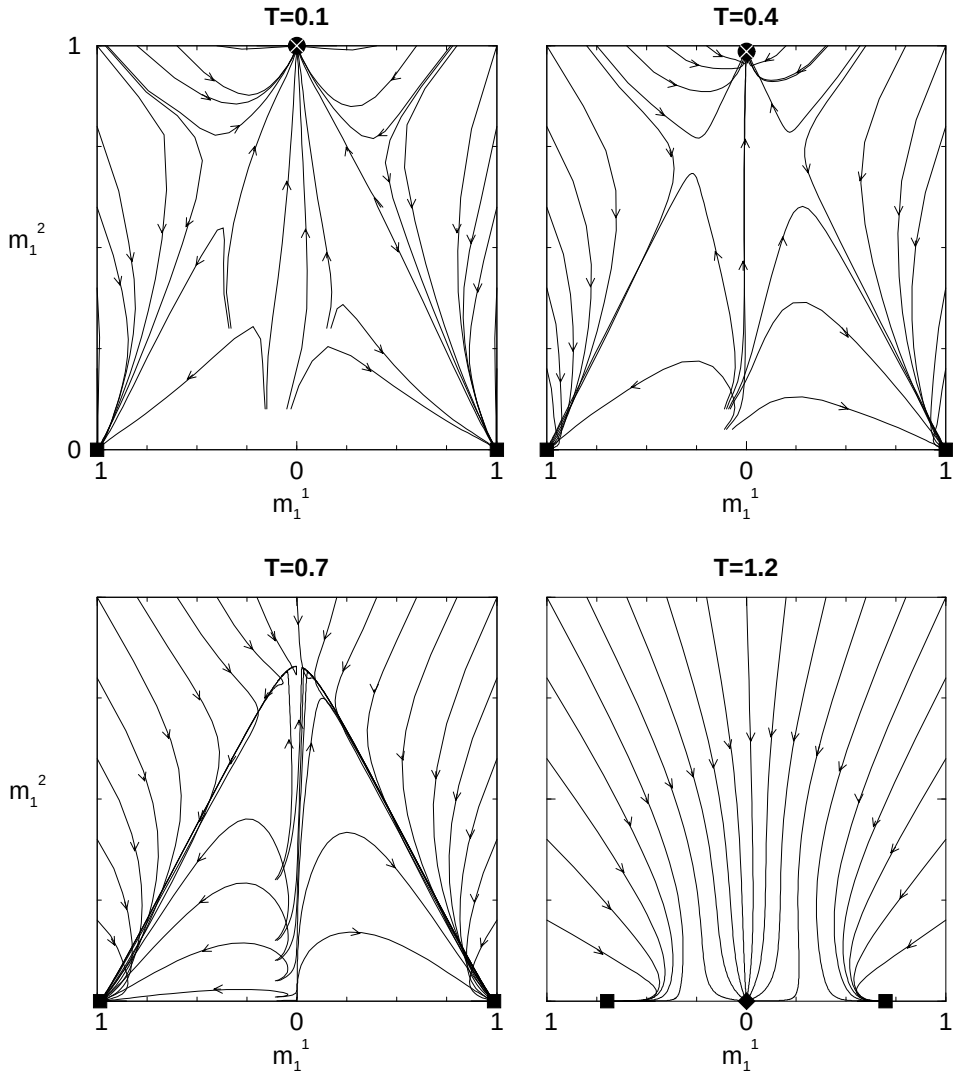

Figure 4. Flow diagrams for the model with linked patterns at different temperatures. Filled symbols stand for different states: a square for *mmm*, a diamond for 000 and a crossed circle for *mm*0.

For higher T this crossed state disappears but the *mmm* states stay in nearly the same place until $T = 1$. Above, the origin is an attractor and the *mmm* states start to move towards the origin (see the diagram for $T = 1.2$). As explained above they do not reach the origin.

The interesting conclusion from these figures is that the state *mmm* has a large basin of attraction. The latter is, of course, somewhat reduced in the temperature region where the stable state 000 also appears. Furthermore, the state *mmm* has a large overlap (recall figure 1) with the embedded patterns.

Since the ATNN model with linked patterns seems to have very good retrieval properties it is worthwhile to derive a $\beta J_1 - \beta J_3$ phase diagram. We first note that the fixed-point

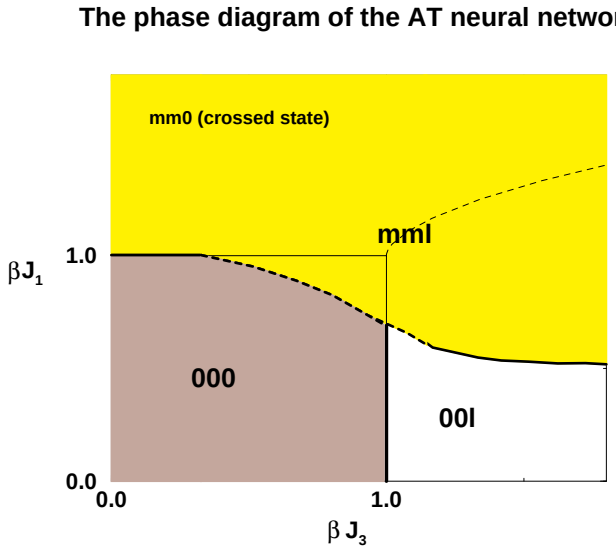

Figure 5. The βJ_1–βJ_3 phase diagram of the ATNN model with linked patterns. The dark grey area represents the 000 phase, the light grey area the full retrieval phase mml and the white area the partial retrieval phase $00l$. Heavy full curves indicate continuous transitions, heavy broken curves discontinuous ones.

equations (6) for the simple Mattis states have the same form as those for the mean-field Ashkin–Teller model. Because these states are always the global minima of the free energy they determine the transition lines. Of course the meaning of the phases is different from the standard Ashkin–Teller model. For the special case of one embedded pattern, i.e. $p = 1$, with $\xi_i^1 = \eta_i^1 = 1$ both models are completely equivalent.

The ATNN βJ_1–βJ_3 phase diagram (for low loading of linked patterns) is presented in figure 5. We distinguish the following phases. The dark grey area is the paramagnetic 000 phase. The light grey area is the full retrieval phase (for linked patterns) described by the simple Mattis state mml ($m \neq l$ when $J_1 \neq J_3$). The white area represents a partial retrieval phase, i.e. only patterns embedded in one part of the network are recalled by the state $00l$. The (heavy) full curves indicate second-order transitions, the (heavy) broken curves discontinuous ones. We remark that the 000 state exists as a minimum up to the light full curves, but outside the dark grey region its energy is higher than the energy of the mml state. In part of the full retrieval phase, namely in the upper half of the phase diagram, the crossed state $mm0$ exists. It is stable in the area above the light full and light broken curves.

5. Conclusions

We have analysed a neural network version of the Ashkin–Teller spin-glass model for low loading of patterns. Both the thermodynamic and dynamic properties have been considered, especially for Mattis states which are the most interesting states from the point of view of retrieval. Fixed-point equations as well as flow equations for the relevant order parameters have been derived. Numerical results have been discussed illustrating the typical behaviour of the network.

The following main conclusions can be drawn. For unlinked embedded patterns the

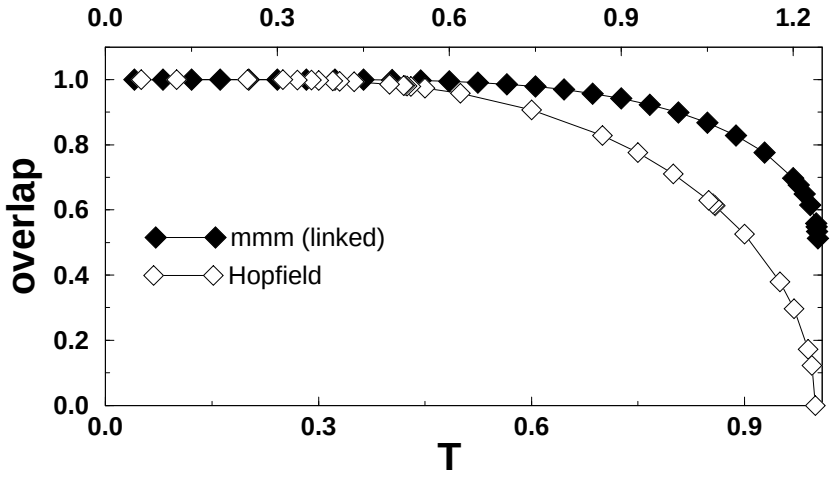

Figure 6. The overlap as a function of a rescaled T for the state mmm in the ATNN model with linked patterns (filled diamond) versus the overlap for the Mattis state in the Hopfield model (empty diamond). Temperature scales refer to the Ashkin–Teller model (top) and the Hopfield model (bottom).

behaviour of the model is much richer than in the case of the standard Hopfield model in the sense that many different forms of stable Mattis states are possible. These states exist up to $T = 1$ where a continuous transition occurs from the retrieval phase to the paramagnetic phase. The corresponding flow diagrams are quite complicated but verify the existence of this many attractors. However, none of these retrieval states has a bigger overlap than the Mattis states of a corresponding Hopfield model. Hence the inclusion of the four-neuron interaction term does not particularly improve the quality of retrieval.

For linked embedded patters interesting new features show up. The most important one is that stable Mattis states of the form mmm appear. They have a very big overlap with the embedded patterns, meaning that the pairs of patterns which are linked by the four-neuron term are retrieved with a very high accuracy. Furthermore, they exist up to $T = 1.213$ and have a large basin of attraction. For temperatures $1 \leqslant T \leqslant 1.213$ both these Mattis states and the paramagnetic solution are local minima of the free energy such that their basin of attraction is somewhat reduced. To verify then that this large overlap m is not just a rescaled overlap of the corresponding Mattis state of a corresponding Hopfield model we have made a comparison in figure 6. We clearly see the difference in shape in favour of the ATNN. Further details of additional features of the ATNN model are given in a $\beta J_1 - \beta J_3$ phase diagram (see figure 5).

In brief, the linked pairs are retrieved easily and with a high precision (simple states) and the unlinked pairs may be retrieved (crossed states), but always with lower precision than that of the linked ones. It is important to stress that the patterns which are linked can be completely different. In principle, they are independent.

Acknowledgments

This work has been supported in part by the Research Fund of the K U Leuven (grant OT/94/9). The authors are indebted to Marc Van Hulle of the Neurophysiology Department of the K U Leuven for interesting discussions concerning the possible biological relevance

of this model. PK would like to thank Professor G Kamieniarz for encouragement to study neural networks. Both authors acknowledge the Fund for Scientific Research-Flanders (Belgium) for financial support.

References

[1] Hopfield J J 1982 *Proc. Natl Acad. Sci., USA* **79** 2554
[2] Gerl F and Krey U 1994 *J. Phys. A: Math. Gen.* **27** 7353
[3] Bollé D, van Hemmen J L and Huyghebaert J 1996 *Phys. Rev.* E **53** 1276
[4] Kühn R and Bös S 1993 *J. Phys. A: Math. Gen.* **26** 831
[5] Bollé D, Rieger H and Shim G M 1994 *J. Phys. A: Math. Gen.* **27** 3441
[6] Christiano P L and Goulart Rosa Jr S 1986 *Phys. Rev.* A **34** 730
[7] Moreira J V and Christiano P L 1992 *Phys. Lett.* A **162** 149
[8] Moreira J V and Christiano P L 1992 *J. Phys. A: Math. Gen.* **25** L739
[9] Nobre F D and Sherrington D 1993 *J. Phys. A: Math. Gen.* **26** 4539
[10] Viana L and Martinez C 1995 *J. Physique* I **5** 573
[11] Provost J P and Vallee G 1982 *Phys. Rev. Lett.* **49** 409
[12] Amit D J, Gutfreund H and Sompolinsky H 1985 *Phys. Rev.* A **32** 1007
[13] Bollé D and Mallezie F 1989 *J. Phys. A: Math. Gen.* **22** 4409
[14] van Hemmen J L, Grensing D, Huber A and Kühn R 1986 *Z. Phys.* B **65** 53
[15] Coolen A C C and Ruijgrok TH W 1988 *Phys. Rev.* A **38** 4253